

**ABSTRACT**

Climate-change driven effects in the northern hemisphere have potential for wide reaching changes in surface energy balance and ecosystem stability. Observations from the Gravity Recovery and Climate Experiment (GRACE) mission from August 2002 through 2009 and high-resolution geoid model difference from 1999 through 2009, corrected for solid-earth effects, have shown that groundwater storage is changing. Groundwater storage is increasing in watersheds underlain by continuous permafrost: Lena, Yenisei and Arctic coastal plain of Alaska, U.S.A., and Yukon Territory, Canada. The Ob' watershed underlain by nonpermafrost is stable, i.e. no change in its groundwater storage over the observation period. Groundwater storage is decreasing in watersheds underlain by discontinuous permafrost: Mackenzie and Yukon in western North America. We hypothesize that the groundwater storage changes are linked to the development of closed taliks (unfrozen material acting as aquifers) and degradation of permafrost in the continuous permafrost zone and decrease of permafrost lateral extent and development of new open taliks in the discontinuous permafrost zone of the watersheds. The increase in taliks in the continuous and discontinuous permafrost zones may be linked with changes occurring beneath thaw bogs, ponds, lakes and rivers/beds.

**Introduction**

Permafrost is the largest component of the cryosphere (Zhang et al., 1999). Degradation of ice-rich permafrost can lead to significant surface subsidence affecting changes in ecosystem, landscape, and where human habitats are established, significant infrastructure damage (Romanovsky and Osterkamp, 1997; Osterkamp and Romanovsky, 1997). The processes of freezing and thawing, growth and degradation of permafrost, affects the land energy and moisture fluxes (balances) which in turn impact biogeochemical cycles, climate and hydrologic systems (Romanovsky and Osterkamp, 1997; Sergeev et al., 2003; Romanovsky et al., 2007).

In the Arctic terrestrial regions hydrologic processes are controlled by the presence or absence of permafrost and the thermal conductivity of the soil (Romanovsky, 2007; Osterkamp, 1997; Osterkamp and Romanovsky, 1997; Whillans et al., 2007; Zhang et al., 2008). Talik is unfrozen earth material formed by hydrothermal and thermal processes near and beneath the ground surface within permafrost (Woo, 1993). Wildfires in boreal forest and tundra can disturb the underlying permafrost and active layer leading to talik formation (Yoshikawa, et al., 2003). Closed talik can be laterally extensive within permafrost. It can occur beneath lakes and rivers crossing the continuous and discontinuous permafrost zones. Open talik within permafrost connects the ground surface to the unfrozen material beneath permafrost allowing for recruitment of surface water into groundwater storage and loss of groundwater storage into surface water. In winter time, baseflow of rivers in permafrost watersheds is maintained by water leaving groundwater storage (Sergeev et al., 2003; Chapin et al., 2006; Buldovich et al., 2008). Liquid water residing within cold and warm permafrost affects the ground thermal state (Romanovsky and Osterkamp, 2000). The effect is largest near the ground surface and active layer after freeze-up, with stronger thermal gradients at the ground surface and increased heat flux.

Diverse observations across the high-latitude northern hemisphere indicate permafrost temperatures at about 2 meters depth have increased over the twentieth century (Romanovsky et al., 2007). These are correlated well to surface air temperature changes on decadal time scales. Permafrost temperatures in eastern Siberia and northern Alaska have shown the largest magnitude of increases of a few degrees centigrade. Increased surface air temperatures from climate warming over the same period often cannot fully account for increased permafrost temperatures, suggesting that variability in snow cover may be a contributing factor (Osterkamp, 2007). Satellite data suggest that the total area of thermokarst lakes increased up to 12% in the northern continuous permafrost zone in western Siberia through processes of degradation of permafrost, and the number of all lakes increased by 4% over the last 30 years (Smith et al., 2005). However, in the southern discontinuous, sporadic and isolated permafrost zones showed in lake area losses up to 13% and the number of lakes decreased up to 9%.

Global satellite observations from the Gravity Recovery and Climate Experiment (GRACE) have shown to the great promise in detecting secular trends and spatial-temporal variations in land and ocean hydrologic mass balance (equivalent water thickness change) since the operational period beginning in August 2002 and ongoing (Tapley et al., 2004; Wahr et al., 2004, 2006; Chambers, 2006). We investigate the GRACE observations for addressing permafrost, talik and active layer changes in the Lena and Ob'-Irtysh River watersheds regions in northern Alaska and Yukon Territory. In this paper we will show analysis of water equivalent mass changes on the Arctic coastal plain in Alaska.

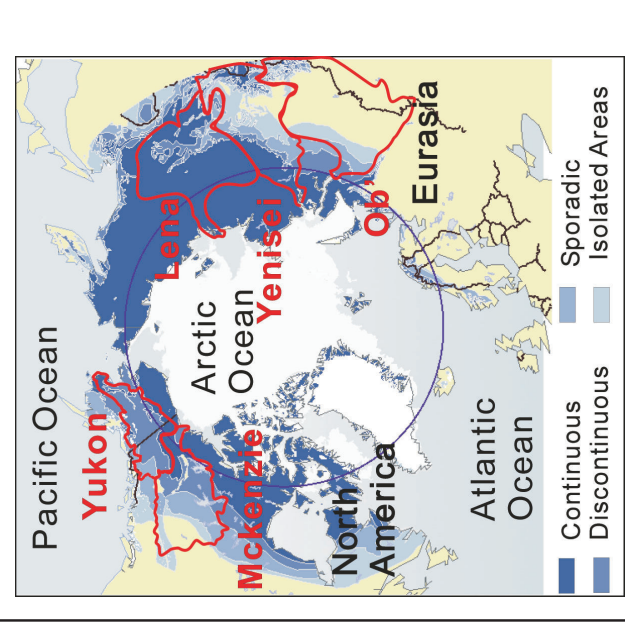


Figure 1. Arctic permafrost, watersheds and distribution of permafrost zones.

**Data Sets**

**GRACE Water Equivalent Mass Changes**

The co-orbiting satellites of the Gravity Recovery and Climate Experiment (GRACE) do not measure the variations of the inter-satellite range (range rate and range acceleration). We use accurate GPS location relative to the International Terrestrial Reference Frame 2005, to estimate values of the time change in spherical harmonic geopotential coefficients,  $\Delta C$  and  $\Delta S$ , in degree and order 120 (the expansion below is complete to degree and order 40) (Chambers, 2006). These are then used in the following formula to estimate movement of water mass:

$$\Delta h(\theta, \lambda, t) = \frac{a^3}{3r_p} \sum_{l=0}^{40} \sum_{m=0}^{l} \frac{(2l+1)}{(l+1)} W_{p,m} \sin(l\theta - (l+m)\omega_{GM}) + \Delta S_{l,m}(t) \sin(m\lambda)$$

$$W = \rho_w \left[ \frac{4\pi a^3}{3} \sum_{l=0}^{40} \sum_{m=0}^{l} \frac{(l+1)}{(2l+1)} \right]$$

$\rho_w$ : Normalized Legendre polynomials

$\Delta C_{l,m}, \Delta S_{l,m}$ : Normalized time-varying Stokes spherical harmonic geopotential coefficients

$a$ : Earth mean radius

$r_p$ : Earth mean radius

$\theta, \lambda$ : Latitude and longitude

$\omega_{GM}$ : Earth rotation rate

$\rho_w$ : Density of water

The GRACE Release 4 Level-3, 300 km smoothing kernel land and ocean monthly grids, from August 2002 through March 2008, were combined to give global coverage. Then, a 1-degree Global Isostatic Adjustment grid (Paulson et al., 2007). Figure 2. Shows the GRACE water equivalent mass change (WEMC) for the terrestrial portion of the Arctic region for the period from August 2002 through March 2007. The error bars show the spatial and/or distribution of the seasonal amplitude of the terrestrial portion of the region. The GRACE water equivalent mass changes on the northern hemisphere show that the permafrost watersheds have a seasonal cycle in September and maximum in May in anti-phase with the mass changes of the Arctic Ocean.

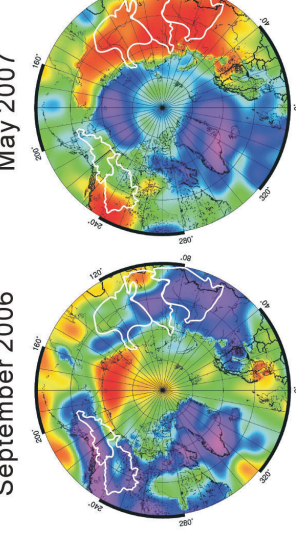


Figure 2. GRACE-derived water equivalent mass changes on the northern hemisphere. The Arctic permafrost watersheds are shown by area-expanses, Yukon and Mackenzie (North America) and Lena, Yenisei and Ob' (Eurasia). The months of September and May are the seasonal minimum and maximum, respectively, of WEMC in the Arctic permafrost watersheds. The strikingly large differences in anti-phase to the seasonal cycle of water equivalent mass changes of the Arctic Ocean.

**High-Resolution Hybrid Geoid Models**

Since the early 1990s the NOAA National Geodetic Survey have been working on development of high-resolution and high-accuracy geoid models as part of the U.S. national mapping and geodetic control network modernization programs (Smith and Milbert, 1999; Smith and Roman, 2001). The efforts centered on producing hybrid geoid models using gravimetric geoid observations (within the U.S. and territorial coastal waters), the U.S. High-Accuracy Reference Network with Global Position System station coordinate determinations and long-wavelength undulations from the Earth Gravity Model 1996 (EGM96) (Lemoine et al., 1998) 360 degree and order 1.5 arc-minute by 15 arc-minute model and realization with respect to the International Terrestrial Reference Frame (ITRF) in the non-tide geoidic reference convention. The first hybrid model 2 arc-minute by 2 arc-minute grid was GEOID-1996 (GEOID96) with a 5.5 cm vertical accuracy. It was followed in 1999 by the 1 arc-minute by 1 arc-minute model GEOID99 with a 4.6 cm vertical accuracy. Hybrid models GEOID03 and GEOID06 followed. The latest efforts have produced GEOID09 which incorporates EGM-2008, a 2159 degree and order 1 arc-minute by 1 arc-minute model (<http://www.ngs.gov/GEOID/USG2009/tech.html>). Early testing was indicating a 1.5 cm vertical accuracy. Furthermore, we use vertical rate data from continuous operating GPS stations in Alaska and Yukon relative to the International Terrestrial Reference Frame 2005 to estimate an adjustment for elastic effects (which are removed from geoid differences in the analysis of water equivalent changes).

**Snow Water Equivalent Changes**

Global snow water equivalent estimates on a monthly basis derive from the NOAA Defense Meteorological Satellite Program by the Special Sensor Microwave Imager (SSM/I), are provided by the National Snow and Ice Data Center ([http://nsidc.org/data/dds/dac/inside\\_0271\\_ease\\_grid\\_swe\\_climatology.gd.html](http://nsidc.org/data/dds/dac/inside_0271_ease_grid_swe_climatology.gd.html)). SSM/I and its predecessor instrument, has been retrieving passive microwave data since 1978. Snow Water Equivalent (SWE) estimates in units of millimeters were derived using the horizontally polarized difference algorithm for the 19 and 37 GHz channels from daily orbit swath acquisitions (Chang et al., 1987). Daily retrievals are averaged to composite monthly estimates. Missing retrievals due to swath coverage gaps are interpolated from neighboring swaths. Sensor resolution is about 69 by 43 square kilometers. The monthly data are gridded in the equal-area Ease-grid projection system at about 25-by-25 kilometer grid intervals.

**Watershed Runoff**

Eurasian and North American based measurements (at gauging stations) of surface water discharge (runoff) in the watersheds were provided by ArcticRIMS (daily) monthly provisional data from 2000 through 2009, R-Arctic-NET (archive monthly data from 1930 through 2000), Arctic Freshwater Systems and the U.S. Geological Survey. Monthly discharge from stations at Kusur (Lena), Igarka (Yenisei), Shtekhard (Ob'), Arctic Red River (Mackenzie), Piton Station (Yukon), Umiat (Colville), and stations near Dead Horse and Prudhoe Bay (Kapuruk and Sigavannitok) were used. The archival periods of the discharged records of each watershed station used varies in total number of years; Kusur covered a period from 1933 through 2006, Igarka covered a period from 1936 through 1999, Shtekhard covered 1960. The monthly discharge records were compared to the prior studies to help identify these anomalies. We also used the monthly runoff from August through July, was chosen as this period coincided with the GRACE time series instead of the typical water year calendar convention. Runoff volume, in cubic meters is converted to water equivalent thickness by dividing by the watershed area in square meters.

**Results**

Figure 3 shows comparisons of area-averaged time series of sample mean and standard deviation, and least-squares regression trends of the Lena, Yenisei, Ob', Yukon and Mackenzie permafrost watershed regions. Take notice of the trends (+ or -) and percentage of permafrost per watershed.

**Eurasian Watersheds**

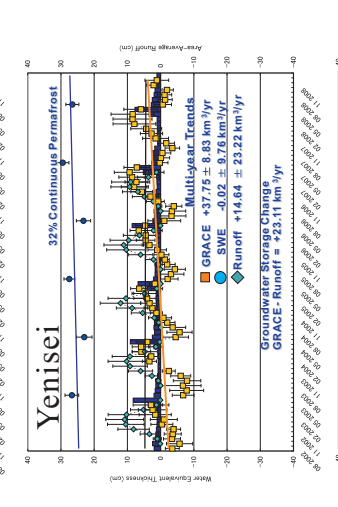
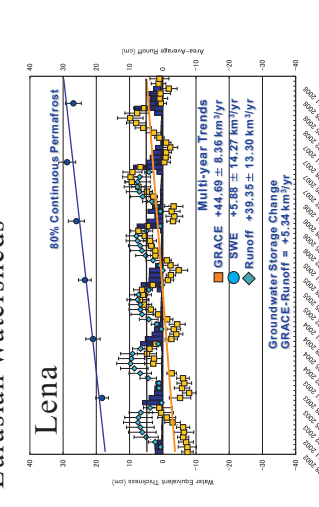


Figure 3. Time series of GRACE (water equivalent mass change), SWE and Runoff. Estimates of groundwater storage change are given.

**GRACE, SSM/I and Runoff Trends and Variations**

GRACE-derived water equivalent mass changes show response to winter water mass loading, derived through SSM/I, and spring water mass unloading derived by watershed runoff in Figure 3 (Muskett and Romanovsky, 2009). Water mass loading precedes the peak in GRACE by about one to two months. Water mass unloading (runoff) in June produces the sharp drop after seasonal peak in the GRACE time series, leading to asymmetric sinusoidal character.

Groundwater storage change is estimated by subtracting runoff trend from the GRACE trend in each watershed:

$$\Delta \text{Groundwater Storage} \approx \text{AGRACE} - \Delta \text{Runoff}$$

This indicates increasing groundwater storage in the Eurasian watersheds and decreasing groundwater storage in the North American watersheds (Muskett and Romanovsky, 2009).

**High-Resolution Geoid Difference Changes in the Alaska Arctic Coastal Plain and the Yukon River Watershed in Alaska, U.S.A., and Yukon Territory, Canada**

To obtain high spatial resolution (1 arc-minute) water equivalent mass changes, we difference the NOAA National Geodetic Survey geoid models GEOID99 (1999 epoch) and GEOID09 (2009 epoch), with adjustment for post-glacial and neotectonic effects by using vertical coordinate GPS-ITRF2005 data at network stations in Alaska and Yukon. The resultant geoid difference map shows the net water equivalent changes from 1999 through 2009 (Fig. 4 on the left). We compare this to a GRACE-difference map (Fig. 4 on the right). The area of the Yukon River watershed is given. The high-resolution geoid-difference area-average mass balance compares closely to the GRACE area-average least-squares trend. Tables 1 and 2 show trends on the Alaska Arctic coastal plain (continuous permafrost) and the Yukon River watershed (mostly discontinuous permafrost).

Table 1. Multi-Year Trends of GRACE (water equivalent mass), SSM/I (snow water equivalent) and Runoff from August 2002 through December 2008. Arctic coastal plain and foothills, and Yukon River watershed.

A. Total Volume Change Rates

Region	GRACE	SSM/I	Runoff
Arctic Coastal Plain	+0.06 ± 0.14 km <sup>3</sup> /a	+0.82 ± 0.36 km <sup>3</sup> /a	-1.14 ± 0.31 km <sup>3</sup> /a
Arctic Foothills	-0.99 ± 0.25 km <sup>3</sup> /a	+0.56 ± 0.42 km <sup>3</sup> /a	-1.14 ± 0.31 km <sup>3</sup> /a
Yukon Watershed	-7.37 ± 2.76 km <sup>3</sup> /a	+7.17 ± 3.51 km <sup>3</sup> /a	+0.08 ± 2.55 km <sup>3</sup> /a

B. Area-Average Thickness Change Rates

Region	GRACE	SSM/I	Runoff
Arctic Coastal Plain	+0.05 ± 0.13 cm/a	+0.78 ± 0.35 cm/a	-1.10 ± 0.31 cm/a
Arctic Foothills	-0.99 ± 0.25 cm/a	+0.56 ± 0.42 cm/a	-1.10 ± 0.31 cm/a
Yukon Watershed	-0.78 ± 0.29 cm/a	+0.63 ± 0.38 cm/a	+0.01 ± 0.38 cm/a

In A. and B. runoff on the Alaskan Arctic coastal plain and foothills is integrated using the discharges from the Colville River (Umiat Station), Kapuruk River (Deadhorse), and Sigavannitok River (Piton Station #3).

Table 2. Groundwater storage Changes from GRACE Trend and Geoid Difference

$\Delta$ Groundwater Storage  $\approx$  AGRACE -  $\Delta$ Runoff

A. Volume Change Rates

Region	GRACE	Groundwater Storage Trend	Geoid Difference
Arctic Coastal Plain	+1.15 ± 0.65 km <sup>3</sup> /a	+2.95 ± 1.97 km <sup>3</sup> /a	+2.95 ± 1.97 km <sup>3</sup> /a
Arctic Foothills	+0.11 ± 0.68 km <sup>3</sup> /a	-0.14 ± 1.37 km <sup>3</sup> /a	-0.14 ± 1.37 km <sup>3</sup> /a
Yukon Watershed	-7.44 ± 3.76 km <sup>3</sup> /a	-7.06 ± 1.04 km <sup>3</sup> /a	-7.06 ± 1.04 km <sup>3</sup> /a

B. Area-Average Thickness Change Rates

Region	GRACE	Groundwater Storage Trend	Geoid Difference
Arctic Coastal Plain	+1.10 ± 0.62 cm/a	+2.83 ± 1.89 cm/a	+2.83 ± 1.89 cm/a
Arctic Foothills	+0.11 ± 0.48 cm/a	-0.13 ± 0.98 cm/a	-0.13 ± 0.98 cm/a
Yukon Watershed	-0.79 ± 0.40 cm/a	-0.78 ± 0.11 cm/a	-0.78 ± 0.11 cm/a

**Groundwater Storage Trend on the Yukon River Watershed**

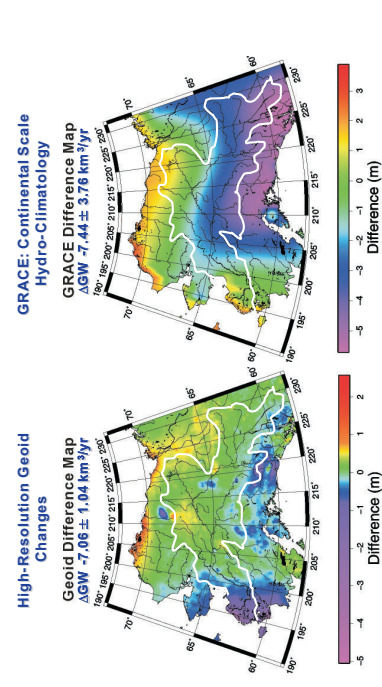


Figure 4. A comparison of spatial variation of groundwater storage changes derived through high resolution (1 arc minute) geoid model difference and the continental scale (1 degree arc) GRACE trend. The high resolution difference includes an adjustment of isotactic solid body effects derived from GPS-ITRF2005 vertical velocities at stations in Alaska and Yukon.

**Conclusions**

In this investigation we have made comparisons of the GRACE water equivalent mass changes (mass balance) with the SSM/I SWE changes, on a nominal monthly basis from August 2002 through December 2008. The discordance of the Least-squares time regression trends of GRACE and SSM/I SWE, lack of correlation of variation, and differences of timing in their seasonal cycles indicate that the source of the GRACE water mass change on the Arctic permafrost watershed regions is not due to surface snow water change. The seasonal loading-unloading of vegetation water content is small, hence the source of the GRACE water mass changes must lie in the subsurface. GRACE-derived groundwater storage shows a water equivalent mass gains in the Eurasian watersheds and water equivalent mass losses in the North American watersheds (Figs. 3 and 4, Tables 1 and 2). We interpret these changes are being facilitated by development and growth of new and existing taliks in the continuous permafrost zone and accompanied by degradation of permafrost in the discontinuous permafrost zone. The development and growth of new and existing taliks is occurring beneath thaw ponds and lakes and rivers/beds. In the continuous permafrost zone increasing groundwater storage capacity. Increasing active layer thickness from thaw sites (on the north water bogs) by position of the talik in the discontinuous permafrost zone (the development of new and existing open taliks, leading to loss of groundwater storage (thaw lake drainage) is hypothesized.

**Acknowledgements**

This work was funded through supporting grants from NASA (NNOG6M48G), the National Science Foundation (NSF ARC0652400 and ARC0856664 projects, Alaska EPCoR NSF award #EPS-071898 and the State of Alaska. The managers and participants in the ArcticRIMS, Arctic Freshwater Systems and U.S. Geological Survey are thanked for providing hydrologic datasets. The Alaska Region Supercomputing Center is thanked for providing computing facilities support. The Japan Aerospace Exploration Agency is thanked for Linux cluster computing support. GRACE data were processed by D.P. Chambers, supported by the NASA Earth Science REASON GRACE Project (<http://dpc.gsfc.nasa.gov>). G. Grosse is thanked for discussion on new thaw pond, lake and spring formation on the Arctic coastal plain of Alaska. R.K. Muskett performed this research at the International Arctic Research Center.

**References**

Buldovich, S., N. Romanowski, G. Tzipenko, D. Sergeev, and V. Romanovsky (2008), Permafrost dynamics within an upper Lena River tributary: Modeled impact of infiltration on the temperature field under a spring, *Geophys. J. Int.*, 171, 1211-1214.

Chambers, D.P. and V.E. Romanovsky (2009), Groundwater storage changes in arctic permafrost watersheds from GRACE and in-situ measurements, *Environ. Res. Lett.*, 4, doi:10.1088/1748-9326/4/04/045009.

Osterkamp, T.E. (2007), Characteristics of the recent warming of permafrost in Alaska, *J. Geophys. Res.*, 112, F02S02, doi: 10.1029/2006JF000578.

Paulson, A., S. Zhong, and J. Wahr (2007), Inference of mantle viscosity from GRACE time series, *Geophys. J. Int.*, 171, 497-508, doi: 10.1111/j.1365-246X.2007.03556.x.

Romanovsky, V.E. and T.E. Osterkamp (1997), Thawing of the active layer on the coastal plain of Alaska, *Perm. & Peri. Process.*, 8 (1), 1-22.

Romanovsky, V.E. and T.E. Osterkamp (2000), Effects of unfrozen water on heat and mass transport processes in the active layer and permafrost, *Perm. & Peri. Process.*, 11 (3), 219-239.

Romanovsky, V.E., T.S. Sazonova, V.T. Babitsky, N.I. Shender, and D.O. Sergeev (2007), Past and recent changes in air and permafrost temperatures in eastern Siberia, *Global & Planet. Change*, 56, 399-413, doi: 10.1016/j.gloplacha.2006.07.023.

Sergeev, D.O., G.S. Tzipenko, V.E. Romanovsky, and N.N. Romanovski (2003), Evolution of mountain permafrost as a result of long-term climate change (in Russian), *Earth Cryosphere*, 7 (2), 15-22.

Smith, D.A., and D.G. Milbert (1999), The GEOID96 high-resolution geoid height model for the United States, *J. Geod.*, 73, 219-236.

Smith, D.A., and D.R. Roman 2001 GEOID99 and G99SSS: 1-arc-minute geoid models for the United States, *J. Geod.*, 75, 469-490.

Smith, L.C., Y. Sheng, G.M. MacDonald, and L.D. Hinzman (2005), Disappearing Arctic lakes, *Science*, 308, 5727, 1429, doi:10.1126/science.1108142.

Tapley, B.D., S. Bettadpur, J.C. Ries, P.F. Thompson, and M.M. Watkins (2004), GRACE measurements of mass variability in the Earth's system, *Science*, 305 (5683), doi:10.1126/Science.1099192.

Wahr, J., S. Swenson, V. Zlotnicki, and I. Velicogna (2004), Time-variable gravity from GRACE: First results, *Geophys. Res. Lett.*, 31, L11501, doi: 10.1029/2004GL019779.

Wahr, J., S. Swenson, and I. Velicogna (2006), Accuracy of GRACE mass estimates, *Geophys. Res. Lett.*, 33, L06401, doi:10.1029/2005GL023503.

White, D., L. Hinzman, L. Alessa, J. Cassano, M. Chambers, K. Falkner, J. Francis, W. J. Gutowski Jr., M. Hollas, J. Max Holmes, H. Huntington, J. Kramo, A. Kliskey, C. Lee, J. McClelland, B. Peterson, T. Scott, R. Rupp, F. Strano, M. Steele, R. Woodgate, D. Yang, K. Yoshikawa, and T. Zhang (2007), The arctic freshwater system: Changes and impacts, *J. Geophys. Res.*, 112, G04S54, doi: 10.1029/2006JG003535.

Woo, M.-K. (1993), Northern Hydrology in Canada's Cold Environments, H.M. French and O. Skjæraker [Eds.], 117-142, McGill-Queen's Univ. Press, Montreal and Kingston, CA.

Zhang, T., R.G. Knowles, J.A. Hegimbottom, and J. Brown (1999), Statistics and characteristics of permafrost and ground-ice distribution in the Northern Hemisphere, *Polar Geograph.*, 23, 132-154.